

A prototype low-background multiwire proportional chamber for measuring alphas and low-energy betas

Z. Ahmed^a, M. A. Bowles^b, R. Bunker^b, S. R. Golwala^a, D. R. Grant^c, M. Kos^b,
R. H. Nelson^{a*}, A. Rider^a, R. W. Schnee^b, D. Sotolongo^a, B. Wang^b, and A. Zahn^a

^a*Division of Physics, Math, and Astronomy
California Institute of Technology
Pasadena, CA 91125, USA*

^b*Department of Physics
Syracuse University
Syracuse, NY 13244, USA*

^c*University of Alberta
Edmonton, AB, T6G 2R3, Canada
E-mail: rhn@caltech.edu*

ABSTRACT: A prototype low-background multiwire proportional chamber (MWPC) was developed to demonstrate the feasibility of constructing a radiopure MWPC to assay materials for alpha- and beta-emitting surface contaminants for future rare-event-search experiments, as well as other scientific fields. We discuss the design features and assembly techniques used to achieve the energy and position resolution for beta and alpha tracks needed for efficient rejection of both intrinsic and external backgrounds. Results from a test setup using a 5.89 keV x-ray source indicate excellent operational stability and a near-ideal energy resolution of 15.8% FWHM. This detector technology promises significant advances in both alpha and low-energy (<200 keV) beta screening.

KEYWORDS: electron multipliers (gas), wire chambers, particle tracking detectors (gaseous detectors), time projection chambers (TPC).

*Corresponding author.

Contents

1. Introduction	1
2. MWPC design and construction	2
2.1 Design requirements	3
2.2 Block-frame design	3
2.3 Spring-loaded feedthroughs	4
2.4 Wire stringing	5
3. Prototype MWPC test setup	6
3.1 Gas handling	7
3.2 Readout electronics	7
4. MWPC performance	9
4.1 Energy resolution and gain	9
4.2 Detector characterization	11
5. Conclusion	13

1. Introduction

Future rare-event searches require unprecedented levels of radiopurity (see *e.g.* [1]). In particular, a troublesome source of contamination results from the noble-gas radioisotope ^{222}Rn , which is sufficiently long lived to pervade laboratory spaces and can lead to the implantation of its long-lived ^{210}Pb and ^{210}Po daughters into or near sensitive detector surfaces. Unfortunately, high-sensitivity detection of the ^{210}Pb 46 keV gamma ray from material surfaces is generally not feasible with HPGe detectors, in part due to its low branching fraction. Furthermore, since these surface contaminants are chemically separated and hence out of equilibrium with the photon-emitting isotopes in the parent ^{238}U decay chain, direct detection of the ^{210}Po alphas or betas from ^{210}Pb or ^{210}Bi is necessary to establish the surface contamination level. Detection of surface betas is necessary for isotopes that can be detected only by the betas they emit (*e.g.*, ^3H , ^{14}C , ^{32}Si , ^{63}Ni , ^{90}Sr , ^{106}Ru , ^{113m}Cd , ^{147}Pm , ^{151}Sm , ^{171}Tm , ^{194}Os , and ^{204}Tl). In addition to its importance for future rare-event searches, more sensitive detection of beta- and alpha-emitting surface contaminants would also benefit archeology, biology, climatology, environmental science, geology, integrated-circuit quality control, and planetary science [2].

A screener intended for low-background detection of alpha and low-energy beta decays has several stringent design requirements:

1. A high-efficiency detection mechanism with good sensitivity to non-penetrating particles from sample surfaces (*e.g.*, a 50 keV beta);
2. A low energy threshold to maximize detection rates from isotopes that emit primarily low-energy betas (*e.g.*, ^{210}Pb);
3. Sufficient energy resolution to permit identification of beta-emitting isotopes by their corresponding beta-spectrum endpoints and of isotopes that emit alphas, internal conversion electrons, or Auger electrons by their characteristic lines;
4. Sufficient position information to allow efficient identification of the source location of contamination and rejection of detector or external backgrounds (*i.e.*, fiducialization);
5. A well-shielded installation to reduce any external backgrounds that cannot be otherwise rejected; and
6. Clean construction from radiopure materials to minimize intrinsic backgrounds.

To achieve these goals, a gaseous time-projection chamber (TPC) is an ideal candidate. Placing a sample directly in the detection medium allows for $\sim 2\pi$ acceptance and very low energy thresholds as there is no dead layer (fulfilling requirements 1 and 2 above). A multiwire proportional chamber [3] (MWPC) has sufficient position and energy resolution for imaging the ionized particle tracks when drifted across the chamber (allowing requirements 3 and 4 to be fulfilled). Passive shielding (requirement 5) of the TPC is reasonably straightforward, and gases may be made sufficiently pure of intrinsic contaminants (partially fulfilling requirement 6). These considerations led to the design of a TPC called the BetaCage [4, 2, 5] with one MWPC near the sample to allow tagging of tracks starting from the sample, separated from a second MWPC by a distance large enough to range out betas up to 200 keV in energy.

The most challenging aspect of the low-background gaseous time-projection chamber is the construction of each radiopure MWPC. The MWPCs must be constructed from affordable materials with good radiopurity to reduce the amount of intrinsic backgrounds. They must be precision machinable to allow uniform wire gain, produce sufficiently low outgassing that electron collection is high and stable with time, and allow connections that produce sufficiently small noise that low thresholds may be achieved. This article documents the design, construction, and operation of a prototype MWPC for use in the planned ultra-low-background screener, the BetaCage.

2. MWPC design and construction

Each MWPC consists of two cathode grids sandwiching a crossed anode grid. The prototype MWPC is a 3-cm thick by 3.8-cm wide frame enclosing a $40.1 \times 40.1 \text{ cm}^2$ active area, while the MWPCs for the proposed screener will have 3-cm thick by 8.3-cm wide frames that each enclose an active area of $76.7 \times 76.7 \text{ cm}^2$; the screener's MWPC frames require additional width to help compensate for the increased strain imposed by their larger wire count. To test the robustness of construction and operation using radiopure materials, the same radiopure materials as planned for the proposed screener are used for the prototype. This section details the choice of materials, the design requirements, and the design and construction of the prototype MWPC.

2.1 Design requirements

The ability to identify beta- or alpha- emitting isotopes imposes only relatively weak requirements on the detector energy resolution and hence the gain uniformity. For alphas, a 10% energy resolution is sufficient to prevent confusion between different alpha lines; other backgrounds in this energy region are expected to be negligible. This 10% energy resolution is more than sufficient to identify beta-decay spectra, since they are identified by their endpoints, which could never be measured better than 10% with small numbers of counts. The isotope ^{210}Pb additionally has internal conversion lines in the 30-46 keV range. At the (dominant) 30 keV line, the intrinsic resolution from carrier statistics is 5.7%, so improvement of the contribution due to gain nonuniformity below 10% is not especially helpful. We therefore require that gain uniformity must be maintained to within $\sim 10\%$.

The gain G of a gaseous proportional chamber is given by the Diethorn formula [6]

$$\ln G = \frac{\ln 2}{\Delta V} \frac{\lambda}{2\pi\epsilon_0} \ln \frac{\lambda}{2\pi\epsilon_0 a E_{\min}(\rho_0) \rho / \rho_0}, \quad (2.1)$$

where λ is the linear charge density on the wire, ϵ_0 is the vacuum permittivity, a is the wire radius, ρ_0 is the density of the gas at STP, ρ is the gas density, and ΔV and $E_{\min}(\rho_0)$ are empirical properties of the gas. The parameter ΔV is the average potential required to produce at least one electron-ion pair, and $E_{\min}(\rho_0)$ is the minimum electric field required.

The expected variations in Eq. 2.1 come from voltage and pressure variations, wire displacements, and wire-diameter variations [7, 8, 9]. The capacitance and potential of the anode with respect to the cathode grids sets λ . A 5% gain variation can result from a 2.5 V (0.2%) high-voltage source variation, a 1.5% wire-diameter variation, or a 100 μm (2%) anode-wire displacement (*cf.* Fig. 1). There is no avalanching at the cathode wires, so their positioning is not as important. Nevertheless, as we detail in §2.3, the prototype’s cathode and anode wires were positioned to within similar tolerances.

2.2 Block-frame design

The MWPC frame is constructed from a high-density plastic called Noryl.¹ The frame was precision machined into four bars, two that hold the anode wires and two that contain the crossed cathode layers. Figure 2 shows a mechanical drawing of the prototype frame. Each layer contains 79 wires with a pitch of 5 mm. The anode-wire plane is also 5 mm from each cathode-wire plane. The four frame pieces were rough-cut, annealed, and finish-cut to a 20 μm (or better) flatness, and then holes for the spring-loaded feedthroughs that hold the wires were drilled. The feedthrus have a tapered shoulder in the middle for seating. The four pieces were arranged as shown in Fig. 2 with stainless-steel alignment pins and bolted together. A 0.5 inch through-hole was drilled into each corner to facilitate connection to either a stand or fieldcage. For the prototype frame, these holes were additionally used to bolt on copper-clad G10 sheets, the purpose of which is discussed in §3.2.

¹Originally developed by GE Plastics in 1966, Noryl is a proprietary amorphous blend of polyphenylene oxide (PPO) and polystyrene (PS) that exhibits excellent hydrolytic and dimensional stability as well as good processability [10]. Screening using a variety of techniques indicates acceptable bulk contamination levels for ^{238}U , ^{232}Th and ^{40}K of ≤ 1 , 3 and 5 mBq/kg, respectively [11].

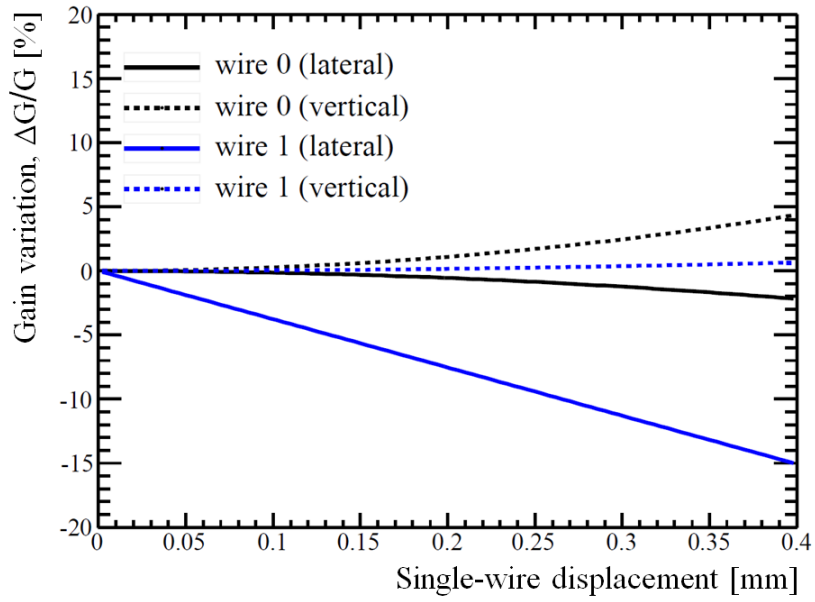


Figure 1. Expected gain variations due to a single wire displacement, both on the displaced wire (wire 0, upper dotted and solid curves) and its nearest neighbor (wire 1, lower dotted and solid curves), where vertical and lateral displacements correspond to deviations out of and in the plane of the MWPC, respectively.

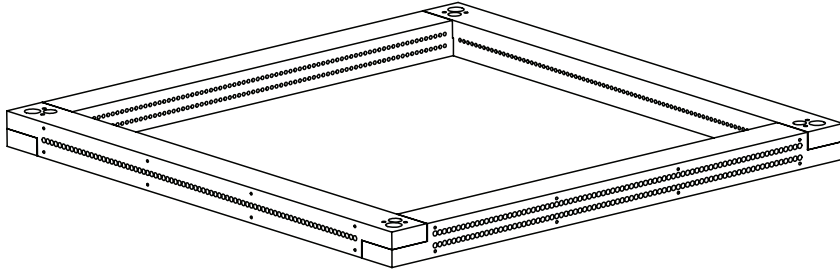


Figure 2. Mechanical drawing of the Noryl block-frame design for the prototype MWPC. The 3-cm thick by 3.8-cm wide frame encloses a $40.1 \times 40.1 \text{ cm}^2$ active area. The anode and cathode layers are defined by the two sides with a single and double row of holes, respectively. There are 79 wires per layer positioned by press-fit, spring-loaded feedthroughs to give a 5 mm inter-wire and -layer pitch.

2.3 Spring-loaded feedthroughs

To prevent gravitational sag, the wires are maintained at uniform tension through the use of custom-design feedthroughs. Each wire is held in place at one end by a spring-loaded feedthrough consisting of two precision-machined brass pieces, a spring, and an annealed copper tube (*cf.* lower drawing in Fig. 3a). At the other end, the wire is held by a simpler, spring-less feedthrough consisting of a single brass piece and an annealed copper tube (*cf.* upper drawing in Fig. 3a). The wires are

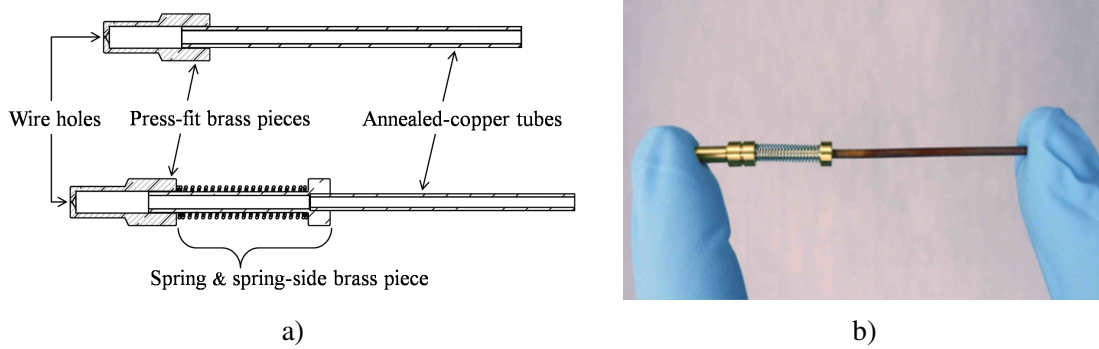


Figure 3. a) Mechanical drawings of the two feedthroughs used to position and tension each wire. Stringing starts by threading the spring-side feedthrough (lower drawing) with a stainless-steel wire and crimping the copper tube (to hold the wire in place). The feedthrough is then press fit into one side of the MWPC frame, and the wire is strung across the frame to the opposing side and threaded through a simpler, spring-less feedthrough (upper drawing), where it is tensioned and finally secured by crimping the second copper tube. b) Photograph of a spring-side feedthrough.

first threaded through the spring-side feedthrough and anchored by crimping its copper tube. The anode (cathode) wires are then threaded through the opposing, spring-less feedthrough, tensioned at 20 g (200 g) using a weight and pulley, and finally secured by crimping the second copper tube. In addition to gripping the wires, the crimps establish electrical connections between the wires and copper tubes, which are used to instrument signal readout and provide high voltage.

As discussed in §2.1, to prevent significant gain variations due to misplacement, a $100\ \mu\text{m}$ tolerance was specified for the positioning of each wire. To achieve this, the feedthroughs were designed to be press-fit into the MWPC frame with a precision in position better than $25.4\ \mu\text{m}$. Further, each press-fit brass piece was designed with an anode (cathode) wire hole with a diameter of $101.6\ \mu\text{m}$ ($177.8\ \mu\text{m}$) centered to better than $25.4\ \mu\text{m}$, thereby accurately guiding each $25.4\text{-}\mu\text{m}$ ($127\text{-}\mu\text{m}$) diameter stainless-steel anode (cathode) wire.² Following fabrication, the prototype MWPC frame and press-fit brass pieces were surveyed, indicating realized tolerances of 20 and $10\ \mu\text{m}$, respectively. The resulting displacement is thus expected to be $<45\ \mu\text{m}$, well within the design specification described in §2.1 to maintain uniform gain.

2.4 Wire stringing

The MWPC wires were strung by hand using a multi-step procedure (see also App. C in [13]). As demonstrated in Fig. 4a, each wire was guided through opposing feedthrough holes using a long aluminum rod inserted through the holes to pull the wire back through the frame. The end of the wire at the spring-side was then threaded through the fully assembled spring-side feedthrough with the help of suction on the end of its copper tube (via a weak vacuum). With the threaded feedthrough held in place by a custom jig containing a pneumatic crimp tool, the feedthrough's copper tube was crimped, and the whole feedthrough was carefully press fit into the frame. The opposite end of the wire was then inserted into the spring-less feedthrough, also with the help of

²Gauge 50 (36) type 304 stainless-steel wire from the California Fine Wire Co. was used for the anode (cathode) [12].

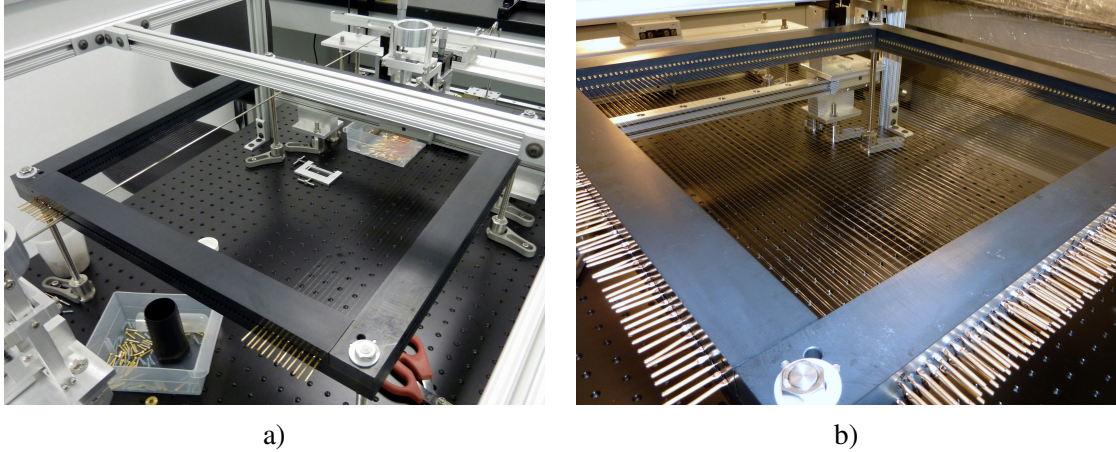


Figure 4. a) Photograph of the setup used to string the prototype MWPC frame. During the stringing process, the frame was secured to an optical table via threaded rods at each of the four corners and surrounded by a T-slotted aluminum frame to help protect the wires. Custom-design fixtures for positioning a crimping tool were located on rails just outside opposing sides of the anode frame pieces. An aluminum rod was used to unspool wire from the far side and through two opposing frame holes. After anchoring the wire to the frame via the spring-side feedthrough (near side), it was tensioned using an aluminum bar attached to a low-friction slide (top of photo behind crimping fixture) and secured via the spring-less feedthrough. The frame was rotated 90° in order to string the cathode layers. b) Photograph of the fully-strung MWPC prototype. Assembly was completed by crimping fly-wires to the copper tubes along the outer edges of two adjacent sides of the frame. The fly-wires were connected to custom circuit boards mounted directly to the frame.

suction. Before tensioning the wire, the feedthrough was carefully press fit into the frame and a similar crimping jig was moved into place. A custom-machined aluminum bar with the same hole pattern as the frame was affixed to a nearly frictionless slide. A weight, hanging from the bar using a low-friction pulley, provided tension to the wire, at which point the spring-less feedthrough's copper tube was crimped. It took 6 minutes to string a single wire. The fully strung prototype MWPC is shown in Fig. 4b.

The final step in the MWPC assembly was to affix custom printed circuit boards (PCBs) to two edges of the frame. Fly-wires crimped to the ends of the copper tubes were then attached to the PCBs, thereby establishing electrical connections from the MWPC wires to coaxial cabling (soldered directly to pads on the PCBs). This final step will be different for the planned screener; the G10-based PCBs used in the prototype will be replaced with (more expensive) Cirlex,³ a material widely used in dark matter experiments because of its radiopurity [15], low outgassing rate, and well-known mechanical properties (see *e.g.* [16]).

3. Prototype MWPC test setup

In this section, we briefly review the experimental configuration used to test the energy response and operational stability of the prototype MWPC. The completed frame was placed inside a stainless-steel pressure vessel that was connected to a rudimentary gas-handling system, providing a con-

³Cirlex is an adhesiveless sheet material made from DuPont's Kapton polyimide and offered by Fralock [14].

trolled space for the introduction of a drift gas. Electrical connections were made via SHV vacuum feedthroughs attached to the bottom of the vessel, enabling application of an electric field and signal readout.

3.1 Gas handling

Ultimately, the planned screener will be operated with a neon-methane mixture. Neon is preferred because it has no naturally-occurring long-lived radiocontaminants, making it an ideal medium for low-background screening. Additionally, its stopping power is low enough that the trigger MWPC can be thick enough (1 cm) to make assembly straightforward. For tests with the prototype, the more common (and less expensive) P-10 gas—a mixture of 90% Ar and 10% CH₄—was chosen for the detection medium. The average energy loss of an incident particle to create a single electron-ion pair in this mixture is $W = 26$ eV [7]. Therefore, 38.5 ± 2.6 electron-ion pairs are created per keV of deposited energy.⁴

The gas-handling system consisted of a gas cylinder, an input manifold, and a turbo and roughing pump. The pressure vessel was first pumped down to a vacuum between 10^{-3} – 10^{-5} Torr before filling with room-temperature P-10 gas (purchased premixed). The P-10 mixture was allowed to flow freely into the chamber and was monitored with an analog relative-pressure gauge. Flow was terminated (by hand) once a slight overpressure of 0.5 psig was achieved, thus minimizing contamination of the detection gas due to laboratory air leaking into the pressure vessel. Since the gas gain varies only linearly with pressure, this somewhat crude introduction of P-10 gas was sufficient to characterize the MWPC response; as shown in Fig. 8, the gain varied by (at most) a few percent due to the resulting pressure variation. Eventually, an MKS 902 piezoelectric transducer [18] was added to monitor pressure to an accuracy of 1%, permitting the measurements discussed in §4.2.

3.2 Readout electronics

A simple single-channel data acquisition (DAQ) was used to test the performance of the MWPC. The three central anode wires were ganged together (on the PCBs described in §2.4) and read out as a single channel. The remaining anode wires were held at the same potential—ranging from 1900–2250 V for most tests—but were otherwise uninstrumented. During standard operations, the anode was biased to 2100 V, while the cathode planes were kept at a small, 100 V potential to create a 2 cm drift region between the cathode and the grounded G10 sheets bolted to the MWPC frame (as indicated in Fig. 5).

The anode and cathode potentials were maintained by a Bertan Model 375P high-voltage power supply [19], designed specifically for MWPC operation. Since the gas gain is proportional to (λ^λ) , the voltage source must be extremely stable to prevent significant gain variations. The high voltage was additionally conditioned by a two-stage low-pass filter with a 72 Hz cut-off frequency. All MWPC wires were biased with one end floating.

A Cremat CR-111 [20] two-stage charge amplifier was used to shape and amplify signals from the central three anode wires. Its first stage is a high-gain integrating amplifier with feedback resistance $R_f = 10$ M Ω and feedback capacitance $C_f = 15$ pF, yielding a 150 μ s output-pulse decay time. The second stage is a low-gain amplifier intended to drive an output current through a coaxial

⁴The Fano factor in P-10 gas is 0.17 [17].

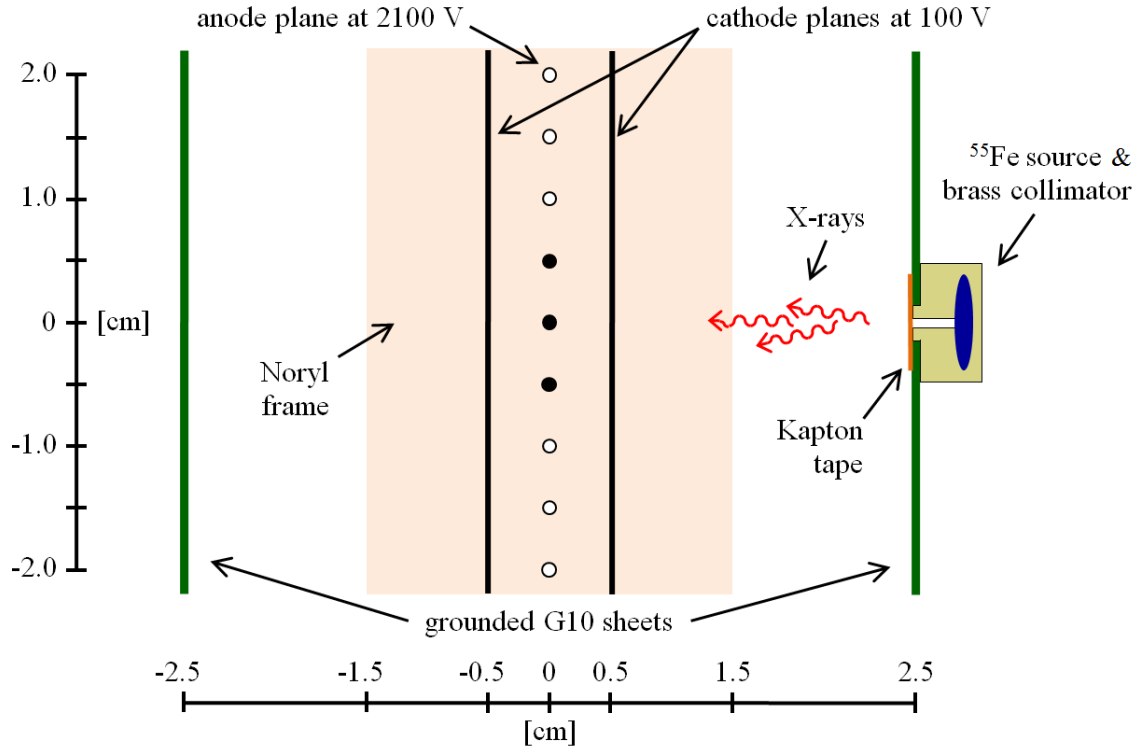


Figure 5. Diagram of the drift-field and ^{55}Fe -source configuration used to test the prototype MWPC, highlighting the center of its crossed wire planes and drawn to scale. The three central anode wires (dark dots) were read out as a single channel, while the others (light dots) were biased but otherwise uninstrumented. The shaded region corresponds to the Noryl frame's 3 cm thickness. Except for the Fig. 6 spectrum, all tests were made with the copper-clad G10 sheets attached to the Noryl frame via 1-cm thick nylon spacers, yielding a 2 cm drift region for ionization electrons created between the Kapton tape and right-side cathode wires (as shown). The data featured in Fig. 6 were obtained with an earlier configuration in which the G10 sheets were bolted to the frame without spacers, resulting in a 1 cm drift region. This difference should have little to no effect on the energy response.

transmission line. The total gain of the CR-111 is 0.13 V/pC. The rise time of the output pulses, barring additional input capacitance, is 3 ns.

A National Instruments PCI-5105 ADC [21] was used to digitize the CR-111 output with 12-bit resolution at a rate of 60 MS/s. The PCI-5105 offers both triggered- and continuous-digitization modes, where the former uses an internal comparator and the latter can be configured to yield ~ 1 -s long traces. In triggered mode, the maximum acquisition rate is ~ 10 Hz and is nearly saturated by cosmic-ray shower activity and other ambient backgrounds. Consequently, it turned out to be more practical to search for test pulses by scanning for local maxima within a narrow window across long, untriggered traces. To reduce high-frequency noise, a 6th-order Butterworth filter with a 10 kHz cut-off frequency was applied to the raw traces. This technique was used to measure pulse-height spectra, study pulse pile-up, and to estimate absolute rates.

With this setup, a gas gain of 10^4 should produce pulses of 8.0 mV/keV. The Cremat amplifier noise in this configuration has been measured to be 2.5 mV (referred to amplifier output), which

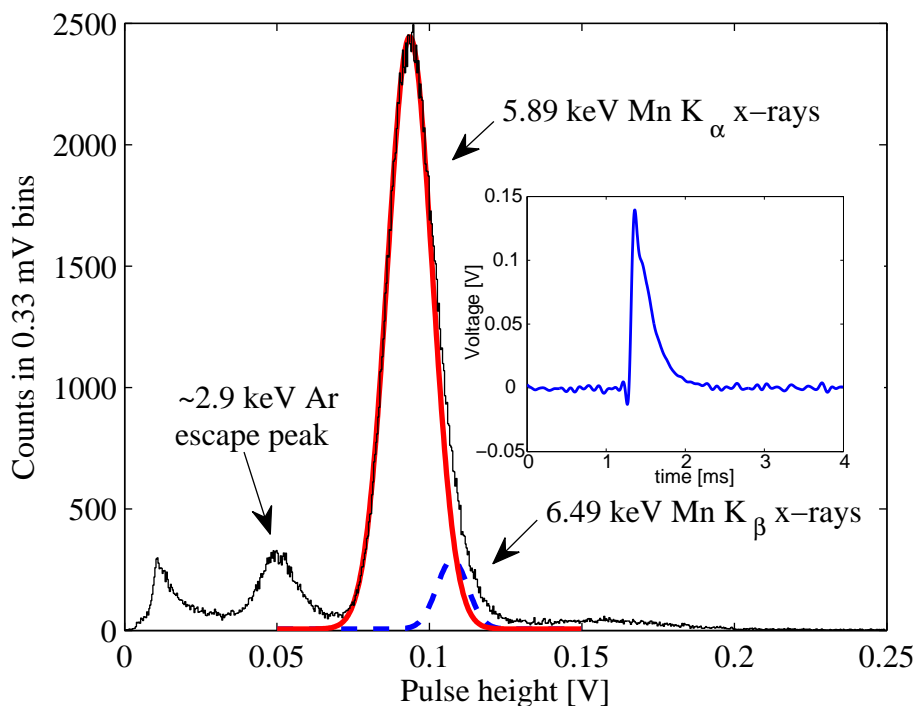


Figure 6. Pulse-height spectrum recorded with the prototype MWPC when exposed to an ^{55}Fe source. The Mn K-shell x-rays are observed as a single peak with the addition of an ~ 2.9 keV Ar escape peak. A combination of two Gaussians and a linear background was fit to the region with pulse heights $\gtrsim 0.07$ V, where the means of the two Gaussians were constrained to have the expected 6.49-to-5.89 ratio. This hypothesis has a $\chi^2/\text{d.o.f.} = 502/487$ and yields a FWHM resolution of 15.8% for the 5.89 keV peak, close to the minimum possible value of 12.8%. The best-fit Gaussians for the 5.89 keV (solid) and 6.49 keV (dashed) peaks are shown independently without the linear background. Inset: A typical ~ 6 keV pulse following application of a digital low-pass filter and with the anode and cathode potentials set to 2100 and 100 V, respectively.

corresponds to 0.439 keV. The relative contributions of electronic noise and statistical fluctuations are discussed in §4.1.

4. MWPC performance

To assess the performance of the prototype MWPC, several tests were conducted using x-rays from an ^{55}Fe source. Energy resolution and gain were measured as functions of voltage, pressure, and time, and estimates of the Diethorn parameters ΔV and E_{min} were extracted.

4.1 Energy resolution and gain

^{55}Fe decays via electron capture with a half-life of 2.73 years, producing Mn K-shell x-rays at 5.89 and 6.49 keV. The 5.89 keV x-rays have almost an order of magnitude larger branching fraction than the 6.49 keV x-rays. Further, in gaseous detectors the two energies tend to be indistinguishable due to the relatively large intrinsic energy resolution. The source activity as of February 1, 2012 was

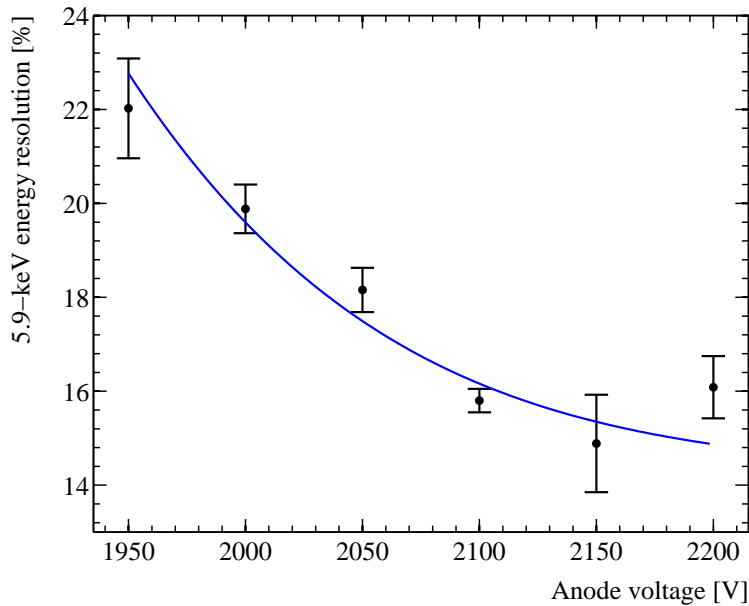


Figure 7. Measured energy resolution of the 5.89 keV peak as a function of voltage. The resolution degrades with decreasing bias voltage due to an increasing contribution from a gain-dependent electronic-noise term in the overall resolution function (*cf.* Eq. 4.1). The data (dots with 1σ error bars) were taken in 1-minute intervals except at 2100 V for which a 20-minute acquisition was performed. We find best-fit estimates ($\chi^2/\text{d.o.f.} = 8.5/4$) for the FWHM intrinsic and electronic-noise resolutions of $14.2 \pm 0.8\%$ and $7.6 \pm 1.0\%$, respectively.

26.5 μCi . Its active region is ~ 3 mm in diameter. The choice of argon as the detection gas also introduces a 2.9 keV escape peak to the spectrum. When an x-ray ionizes a K-shell electron in Ar, the Ar atom emits an Ar K-shell x-ray with an energy of 3 keV due to the filling of the K-shell vacancy. This 3 keV x-ray has a longer absorption length than a higher-energy x-ray and so may escape the detection region, resulting in a peak 3 keV below that of the primary x-ray. This is actually a collection of lines, making it difficult to fit for the energy resolution.

The ^{55}Fe source was centered on the MWPC immediately outside the drift region external to the copper-clad G10 ground plane (*cf.* Fig. 5). The source was affixed to a 3.2-mm thick gold-plated copper collimator with a 1-mm diameter circular aperture. The front of the collimator was covered with a thin layer of Kapton tape to prevent electrons created outside the drift region from entering it.

To search for the 5.89 keV x-rays, a voltage scan was performed near the potential expected to yield a 10^4 gas gain. These scans were taken both with and without the source present to confirm that any spectral features could indeed be attributed to the ^{55}Fe source. Once the peak was located, the voltage was tuned to bring the x-ray and escape peaks well above the noise threshold. Figure 6 shows the pulse-height spectrum of an ^{55}Fe -source run taken with anode and cathode potentials of 2100 and 100 V, respectively. The Mn K-shell x-rays are observed along with an ~ 2.9 keV escape peak. The best-fit mean of the 5.89 keV peak was used to calibrate the energy scale.

The 5.89 keV peak fit featured in Fig. 6 yields a near-ideal FWHM energy resolution of 15.8%.

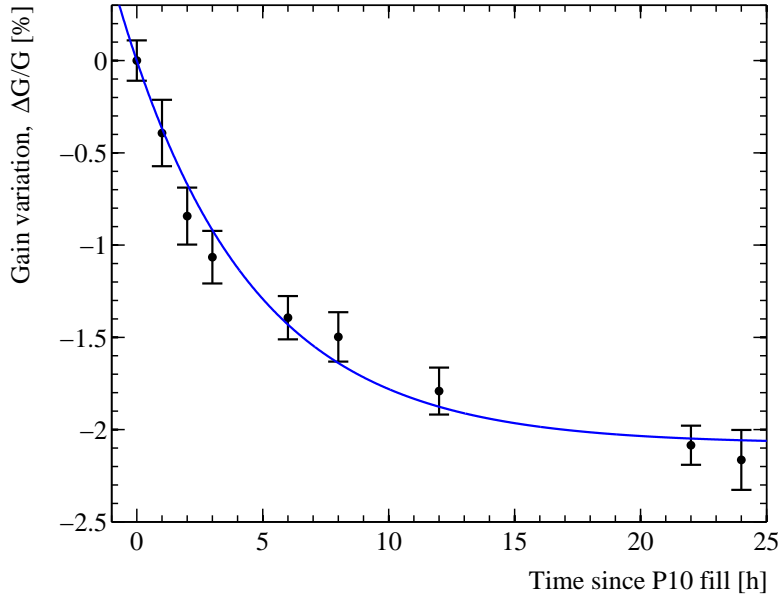


Figure 8. Stability of the gain (vs. time) following a P-10 gas fill. A series of ^{55}Fe -source runs were taken over the course of a day, with the means of the resulting 5.89 keV peaks indicating a slight, few-percent degradation in gain (dots with 1σ error bars). Attributed to drift-gas contamination due to outgassing from detector materials, the degradation is well-fit by a two-parameter exponential form (cf. Eq. 4.2) with a $\chi^2/\text{d.o.f.} = 4.6/7$, an amplitude $A_{\text{stability}} = -2.08 \pm 0.09\%$, and a $1/e$ decay time $\tau_{\text{stability}} = 5.1 \pm 0.7$ h.

As demonstrated in Fig. 7, the resolution improves as expected with increasing gas gain, given by the expected functional form

$$\frac{\text{FWHM}}{\bar{G}} = \sqrt{\text{FWHM}_0^2 + \frac{\text{FWHM}_{\text{elec}}^2}{\bar{G}^2}}, \quad (4.1)$$

where \bar{G} is the pulse-height gain normalized to 2100 V, FWHM_0 is the intrinsic resolution at 5.89 keV, and $\text{FWHM}_{\text{elec}}$ is the electronic-noise contribution. We find $\text{FWHM}_0/5.89 \text{ keV} = 14.2 \pm 0.8\%$ and $\text{FWHM}_{\text{elec}}/5.89 \text{ keV} = 7.6 \pm 1.0\%$, where the latter agrees with the electronic noise given in §3.2. The measured intrinsic resolution is only slightly larger than the minimum theoretical value of 12.8% from electron-ion pair and avalanche statistics, implying a contribution due to gain non-uniformity and/or gas contamination $< 7\%$, well within required specifications. (We note that the theoretical FWHM_0 is expected to scale as $1/\sqrt{E}$ while $\text{FWHM}_{\text{elec}}$ is independent of E .) Furthermore, we expect both the intrinsic uncertainty and the electronics noise to improve with upgrades to the electronics, gas-handling system, and a position-corrected analysis.

4.2 Detector characterization

To assess the prototype’s operational stability, several short ^{55}Fe -source runs were recorded over the course of a day subsequent to a P-10 gas fill. Figure 8 shows the resulting stability of the gain, measured by the location of the 5.89 keV peak, as a function of time. The observed gain variation

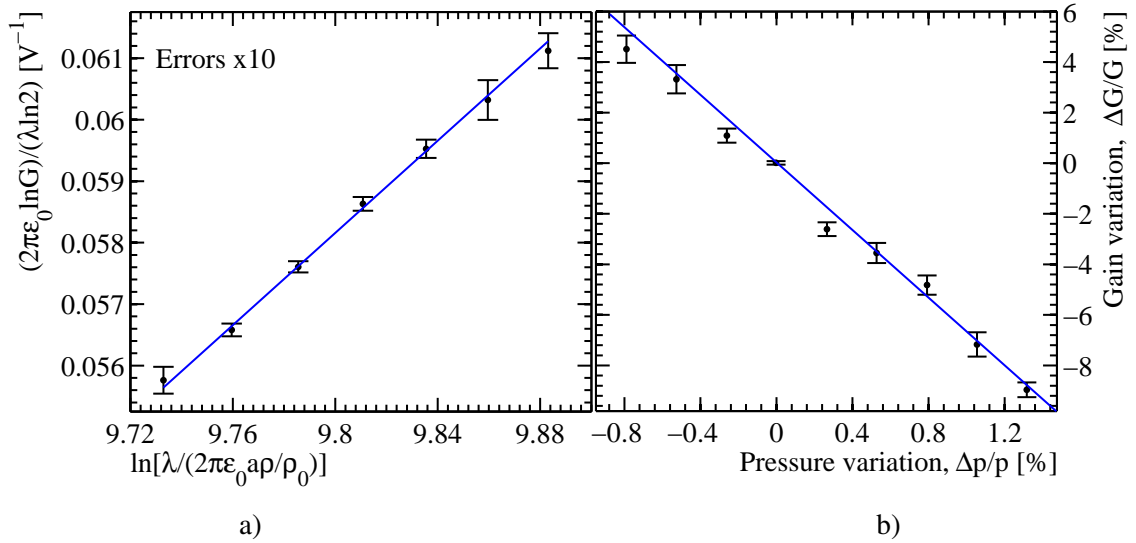


Figure 9. a) Test of the Diethorn formula for gas gain in a proportional chamber, where Eq. 2.1 has been rearranged to yield a linear relationship with varying anode voltage (dots with exaggerated 1σ error bars). An estimate of the Diethorn parameters is extracted with a linear fit; $\Delta V = 26.7 \pm 0.6$ V and $E_{\min} = 38.3 \pm 1.3$ kV/cm, in agreement with expectation. b) Gain variation, as measured with 5.89 keV x-rays, as a function of pressure change (dots with 1σ error bars). The Diethorn formula predicts a slope of -6.5 ± 0.3 that is confirmed by a best-fit slope of -6.7 ± 0.3 .

is well-fit by an exponential trend:

$$\frac{\Delta G}{G} = A_{\text{stability}} \left(1 - e^{-t/\tau_{\text{stability}}} \right), \quad (4.2)$$

where t is time since the P-10 gas fill. The best-fit amplitude $A_{\text{stability}} = -2.08 \pm 0.09\%$, and the best-fit decay constant $\tau_{\text{stability}} = 5.1 \pm 0.7$ h. The primary reason for the gain drift is attributed to outgassing from the various detector components. For the planned screener, the detection gas will be continuously circulated through a SAES MC190-902F MicroTorr purifier [22] and a (custom-design) cooled-carbon radon trap [11] to help remove outgassed contaminants and thus further improve gain stability.

The Diethorn parameters ΔV and E_{\min} were estimated with a fit to $(2\pi\epsilon_0 \ln G)/(\lambda \ln 2)$ as a function of $\ln|\lambda/(2\pi\epsilon_0 a\rho/\rho_0)|$ (cf. Fig. 9a), where the variation in the charge density results from varying the high voltage. This linear relationship allows for easy extraction of the Diethorn parameters; $\Delta V = 26.7 \pm 0.6$ V and $E_{\min} = 38.3 \pm 1.3$ kV/cm, with expectations of 23.6 ± 5.4 V and 48 ± 3 kV/cm, respectively [23].⁵ All uncertainties are statistical at 1σ confidence.

An additional check on the performance of the MWPC is to vary the pressure and monitor the corresponding change in gain. Figure 9b shows this measurement, again using the location of the 5.89 keV peak to track the gain. This linear relationship between gain and pressure is expected to have a slope of -6.7 ± 0.3 [7]. The best-fit slope to the data in Fig. 9b is -6.5 ± 0.3 .

⁵Historically, there is a wide range of measured E_{\min} values that encompass our estimate [7].

Table 1. Comparison of several expected gas parameters with those measured with the prototype MWPC. As outgassing is hard to predict, there is no expectation for the two stability parameters. All uncertainties are quoted at 1σ confidence.

parameter	description	expected	measured	units
FWHM_0	intrinsic resolution @5.89 keV	12.8	14.2 ± 0.8	%
$\text{FWHM}_{\text{elec}}$	electronic-noise resolution	7.5	7.6 ± 1.0	%
$A_{\text{stability}}$	gain-stability amplitude		-2.08 ± 0.09	%
$\tau_{\text{stability}}$	gain-stability $1/e$ decay time		5.1 ± 0.7	h
E_{min}	Diethorn minimum electric field	48 ± 3	38.3 ± 1.3	kV/cm
ΔV	Diethorn electron-ion potential	23.6 ± 5.4	26.7 ± 0.6	V
$\frac{\partial(\Delta G/G)}{\partial(\Delta p/p)}$	gain vs. pressure slope	-6.7 ± 0.3	-6.5 ± 0.3	

Table 1 compares the expected values of several characteristic MWPC parameters to those measured with our prototype. Where appropriate, all parameters match to within statistical uncertainties, with E_{min} to within the spread of previous measurements [7]. This is most likely due to slight impurities in the detection gas. As dependence of the gain on this parameter is somewhat muted due to a logarithm, the exact value is not as important as ΔV .

5. Conclusion

A prototype low-background MWPC for the detection of alphas and low-energy betas has been constructed and characterized. This device performs well down to a few keV in deposited energy as shown by the measurement of x-rays produced from ^{55}Fe decays. The MWPC was found to respond with an energy resolution of 15.8% at 5.89 keV, close to the expected 12.8% statistical limit. Further improvements to this resolution will come from planned electronics upgrades to include position information. The gain is stable to $\sim 2\%$ for >1 -day periods and is expected to have negligible instability with a planned upgrade to the gas-handling system that includes a continuous circulation loop with gas purification. Further, gain variations due to pressure changes fall in line with expectation and can be corrected with accurate pressure monitoring. This prototype MWPC has met or exceeded all of its design goals.

Acknowledgments

This work was supported in part by the National Science Foundation (Grants No. PHY-0834453 and PHY-0855525), the Department of Energy HEP division, and the University of Alberta Department of Physics and Faculty of Science. The authors gratefully acknowledge the technical contributions of L. Buda, J. Hanson, G. Lachat, and P. Zimmerman, and the quality-control testing of J. Roberts and M. Minskovsky.

References

- [1] J. A. Formaggio and C. J. Martoff, *Backgrounds to sensitive experiments underground*, *Ann. Rev. Nucl. Part. Sci.* **54** (2004) 361–412. doi:10.1146/annurev.nucl.54.070103.181248.

- [2] R. W. Schnee, Z. Ahmed, S. R. Golwala, D. R. Grant, and K. Poinar, *Screening Surface Contamination with BetaCage*, in *Topical Workshop on Low Radioactivity Techniques: LRT 2006*, vol. 897, pp. 20–25, AIP Conf. Proc., Mar. 28, 2007. doi:10.1063/1.2722063.
- [3] G. Charpak *et al.*, *The use of multiwire proportional counters to select and localize charged particles*, *Nucl. Instrum. Meth.* **62** (1968) 262–268. doi:10.1016/0029-554X(68)90371-6.
- [4] T. Shutt, C. E. Dahl, L. DeViveiros, R. J. Gaitskell, and R. W. Schnee, *Beta Cage: A New, Large-Area Multi-Wire Screening Detector For Surface Beta Contamination*, in *Topical Workshop on Low Radioactivity Techniques: LRT 2004*, vol. 785, pp. 79–83, AIP Conf. Proc., Sep. 8, 2005. doi:10.1063/1.2060456.
- [5] Z. Ahmed, S. R. Golwala, D. R. Grant, M. Kos, R. H. Nelson, R. W. Schnee, and B. Wang, *Status of BetaCage: an Ultra-sensitive Screener for Surface Contamination*, in *Topical Workshop on Low Radioactivity Techniques: LRT 2010* (R. Ford, ed.), vol. 1338, pp. 88–92, AIP Conf. Proc., Apr. 27, 2011. doi:10.1063/1.3590914.
- [6] W. Diethorn, *A methane proportional counter system for natural radiocarbon measurements*, Report NY06628, USAEC, 1956.
- [7] W. Blum, W. Riegler, and L. Rolandi, *Particle Detection with Drift Chambers*. Springer, second ed., 2008.
- [8] F. Sauli, “Principles of Operation of Multiwire Proportional and Drift Chambers.” CERN-77-09, 1977. Lectures given in the Academic Training Programme of CERN 1975–1976.
- [9] G. A. Erskine, *Electrostatic problems in multiwire proportional chambers*, *Nucl. Instrum. Meth.* **105** (1972) 565–572. doi:10.1016/0029-554X(72)90356-4.
- [10] SABIC Innovative Plastics, Pittsfield, MA 01201, USA. www.sabic-ip.com.
- [11] R. Bunker, Z. Ahmed, M. A. Bowles, S. R. Golwala, D. R. Grant, M. Kos, R. H. Nelson, R. W. Schnee, A. Rider, B. Wang, and A. Zahn, “The BetaCage, an ultra-sensitive screener for surface contamination.” To appear in AIP Conf. Proc. for the *Topical Workshop on Low Radioactivity Techniques: LRT 2013*, 2013.
- [12] California Fine Wire Co., Grover Beach, CA 93483, USA. www.calfinewire.com.
- [13] Z. Ahmed. PhD thesis, California Institute of Technology, 2012. cdms.berkeley.edu/Dissertations/ahmed.pdf.
- [14] Fralock Div. Lockwood Ind., Canoga Park, CA 91304, USA. www.fralock.com.
- [15] J. Loach, J. Cooley, A. Cox, A. Poon, K. Adler, M. Bruemmer, K. Nguyen, and B. Wise, “A Community Material Assay Database.” To appear in AIP Conf. Proc. for the *Topical Workshop on Low Radioactivity Techniques: LRT 2013*, 2013. radiopurity.org.
- [16] R. Alon *et al.*, *Operation of a thick gas electron multiplier (THGEM) in Ar, Xe and Ar-Xe*, *JINST* **3** (2008) P01005. doi:10.1088/1748-0221/3/01/P01005.
- [17] G. F. Knoll, *Radiation Detection and Measurement*. John Wiley and Sons, Inc., New York, fourth ed., 2010.
- [18] MKS Instruments, Andover, MA 01810, USA. www.mksinst.com.
- [19] Bertan Model 375P High Voltage Power Supply. Fermilab Electronics Equipment Pool Catalog.
- [20] Cremat, Inc., Watertown, MA 02472, USA. www.cremat.com.

- [21] National Instruments Corp., Austin, TX 78759, USA. www.ni.com.
- [22] SAES Pure Gas, Inc., San Luis Obispo, CA 93401, USA. www.saespuregas.com.
- [23] R. W. Hendricks, *The gas amplification factor in xenon-filled proportional counters*, *Nucl. Instrum. Meth.* **102** (1972) 309–312. doi:10.1016/0029-554X(72)90728-8.